A Novel Comprehensive Verification Method for Multifocal RapidArc Radiosurgery Treatments

by

Michael Henry Niebanck

Graduate Program in Medical Physics
Duke University

Date:_____
Approved:

_____
Mark Oldham, Supervisor

_____
Zhiheng Wang

_____
John Kirkpatrick

Thesis submitted in partial fulfillment of
the requirements for the degree of Master of Science in the
Graduate Program in Medical Physics of Duke University

2012

ABSTRACT

A Novel Comprehensive Verification Method for Multifocal RapidArc Radiosurgery Treatments

Michael Henry Niebanck

Graduate Program in Medical Physics
Duke University

Date:_____
Approved:

_____
Mark Oldham, Supervisor

_____
Zhiheng Wang

_____
John Kirkpatrick

An abstract of a thesis submitted in partial fulfillment
of the requirements for the degree of Master of Science in the
Graduate Program in Medical Physics of Duke University

2012

Copyright by
Michael Henry Niebanck
2012

Abstract

Purpose: Radiosurgery has become a widely used procedure in the treatment of both solid tumors and secondary metastases in the brain. In cases with multiple brain lesions, isocenters are typically set up for each target, a process which can take hours and become very uncomfortable for the patient. Recently, multifocal treatments with a single isocenter have emerged as a solution. With high doses delivered to small regions during radiosurgery, the importance of treatment verification is paramount, especially when delivering high doses to regions off isocenter.

Methods: A 5-arc RapidArc radiosurgery plan with a single isocenter and 5 targets was used to treat a dosimeter placed within a RPC-type head and neck phantom. The treatment was delivered five times at varying prescription doses, depending on the sensitivity of the PRESAGE dosimeter used. The delivered dose distribution was measured using an in-house optical-CT system and compared to the Eclipse-planned dose distribution using dose volume histograms and Gamma analysis.

Results: Reasonable dose agreement was measured between the majority of the dosimeters and the Eclipse plan (80-85% pass rate at 5%/3 mm Gamma criteria). The failing voxels were located on the periphery of the dosimeter at regions of extremely high or low dose, suggesting a dose dependent stability of the PRESAGE formulation.

The formulation with the best temporal stability had a much higher Gamma pass rate of 98% with 3%/2mm criteria.

Conclusions: The potential of accurate delivery of the multifocal SRS plan was demonstrated with one of the three formulations of PRESAGE. While agreement was worse in the other formulations, the problem seemed to be an easily-fixable stability issue, which resulted in improper scaling of doses. Replication of the most stable formulation would provide an excellent tool for verification of radiosurgery treatment delivery and other complex procedures.

Contents

Abstract iv

List of Tables ix

List of Figures x

Acknowledgements xii

1. Introduction 1

    1.1 Overview of Stereotactic Radiosurgery 1

    1.2 Limitations of Radiosurgery 2

    1.3 Multifocal Treatment 2

    1.4 Current Treatment Verification Techniques 3

    1.5 Advantages and role of 3D Dosimetry 4

    1.6 Scope and Aims of this work 4

2. Methods 6

    2.1 Multifocal RapidArc Treatment Planning 6

        2.1.1 iPlan 6

        2.1.2 Eclipse 7

    2.2 Treatment Delivery 7

        2.2.1 Immobilization and Positioning 8

        2.2.2 Arc Set-Up and Beam On 9

        2.2.3 Ion Chamber Absolute Dose Measurements 9

2.3 Optical-CT Scanning and Reconstruction 10
2.3.1 Duke Large-field Optical Scanner (DLOS) 10
2.3.2 Pre and Post Irradiation Scanning 11
2.3.3 Reconstruction Algorithm and Filtering 12
2.3.4 A Novel High Dynamic Range Technique for dark dosimeters 13
2.4 PRESAGE 3D Dosimeters 14
2.4.1 Dose Response 14
2.4.2 Cuvette Irradiation 15
2.4.3 Temporal Stability of PRESAGE 16
2.5 Comparative Analysis of 3D Dose Distributions 17
2.5.1 Registration of measured dose to planned dose 17
2.5.2 Dose Normalization 18
2.5.3 Dose Volume Histogram and Gamma Analysis 19
3. Results and Discussion 20
3.1 PRESAGE sensitivity and temporal stabilities 20
3.1.1 Dose-Response 21
3.1.2 Stability 23
3.2 Dosimeter Studies 25
3.2.1 LS1 Formulation 25
3.2.2 LS2 Formulation 28
3.2.3 D21 Formulation: Preliminary Results 31

3.3 High Dynamic Range scanning 33

4. Conclusions 36

Appendix A: Additional Figures 38

Appendix B: Abbreviation Key 40

References 41

List of Tables

Table 1 Monitor units delivered to the D21 formulation cuvettes 16

Table 2: Overview of PRESAGE dosimeters irradiated in this work 20

Table 3: delivered dose (Gy) to targets: LS1 vs. Eclipse dose 26

Table 4: Delivered dose (Gy) to targets: LS2 dosimeters vs. Eclipse dose 29

Table 5: Gamma passing rates for 3 sets of criteria 30

Table 6: delivered dose (Gy) to D21 vs. Eclipse dose 32

Table 7: Comparison of dose delivery using standard acquisition and high dynamic range acquisition for LS2a dosimeter 34

List of Figures

Figure 1: RapidArc SRS plan in Eclipse; the 5 arcs are shown in red and the five targets are labeled 7

Figure 2: Novalis Tx at Duke University was used to deliver the SRS treatment 8

Figure 3: Head and neck phantom with target positioning paper and frame..... 9

Figure 4: Diagram of DLOS system [20] 11

Figure 5: MATLAB-based reconstruction GUI; pre and post scans are loaded in in order to generate a sinogram and reconstruct the dose distribution 12

Figure 6: Cuvettes containing PRESAGE irradiated with doses of 0 to 25 Gy..... 15

Figure 7: CERR's registration GUI; PRESAGE dosimeter (right) is registered to the Eclipse distribution (left) by matching the edges 18

Figure 8: Dose response of the D21 formulation (high sensitivity) 21

Figure 9: Dose response of the LS1 formulation (medium sensitivity) 22

Figure 10: Dose response of the LS2 formulation (low sensitivity) 23

Figure 11: Sensitivity change over time of the three formulations 24

Figure 12: Normalized sensitivity change over time of the three formulations 24

Figure 13: Dose profile through central and peripheral targets; Eclipse in yellow and LS1 delivery in blue..... 25

Figure 14: DVH for delivery to LS1 (dashed) vs. Eclipse (solid)..... 26

Figure 15: Eclipse plan compared to LS1 PRESAGE delivery with 3%/2 mm gamma map 27

Figure 16: High dose regions drop over time (left); temporal instability dependent on dose (right) 28

Figure 17: Dose profile through central and peripheral targets..... 29

Figure 18: LS2a dose distribution (left) with gamma maps (3%/2mm, 5%/3mm, 7%/4mm) 31

Figure 19: Dose profile through central and peripheral targets; Eclipse in yellow and D21 delivery in green 31

Figure 20: DVH for delivery to D21 (dashed) vs. Eclipse (solid) 32

Figure 21: Dose dependent temporal instability in D21 33

Figure 22: Linear relationship between counts and shutter value 34

Figure 23: Dose distribution of standard and HDR method (left) and dose profile of standard and HDR methods (right) 35

Figure 24: DVH for LS2a (dashed) vs. Eclipse (solid) 38

Figure 25: DVH for LS2b (dashed) vs. Eclipse (solid) 38

Figure 26: DVH for LS2c (dashed) vs. Eclipse (solid) 39

Acknowledgements

Mark Oldham, PhD

Zhiheng Wang, PhD

Joseph Newton, PhD

Andrew Thomas, PhD

John Adamovics, PhD

Titania Juang

1. Introduction

1.1 Overview of Stereotactic Radiosurgery

The technique of stereotactic radiosurgery was first developed using an orthovoltage X-ray source in the late 1940s and involves the combination of stereotactic positioning of the patient and using ionizing radiation to treat a brain lesion[1].The stereotactic frame is either surgically attached to the patient's skull or attached to the head of the couch. In the latter case, a thermoplastic mask is attached to the stereotactic apparatus and placed over the patient's face to immobilize the patient's head.

The distinction between radiosurgery (SRS) and radiotherapy (SRT) lies in the number of fractions. While SRT utilizes hyperfractionation like most other treatments, SRS uses hypofractionated (1-5 fractions) doses. SRS has been used to treat a wide variety of cranial conditions including primary solid tumors, metastases, and even several benign conditions including pituitary adenoma and acoustic neuroma [1]. While delivering the entire dose in a single fraction results in a high biologically effective dose to the target [2], surrounding normal tissue is at risk to receive the same high dose. Accuracy and steep dose drop-offs are imperative in SRS in order to spare normal tissue [3, 4].

1.2 Limitations of Radiosurgery

Due to the necessary accuracy of stereotactic radiosurgery treatment, the process of patient set-up can take a significant amount of time. Once the patient is immobilized, target positioning paper is used to properly align the isocenter. Next, the position of the patient is verified using cone-beam CT (CBCT) from the on-board imaging system. If multiple brain lesions must be treated, typical treatments would include an isocenter for each lesion [5]. The target positioning paper and frame must be repositioned for each additional isocenter and the set-up verified with CBCT, resulting in increased set-up time and uncomfortably long treatment durations for the patient. In addition to increased set-up time, the actual treatment time is longer than a standard treatment since the dose per fraction is very high. Treatment times for patients with multiple isocenters can exceed an hour, which, in addition to being uncomfortable for the patient, can interfere with other treatments scheduled if the linac is not dedicated to SRS [6, 7].

1.3 Multifocal Treatment

One way to reduce the set-up time is to decrease the number of isocenters of the treatment, since each one requires individual set-up. This can be done by placing the isocenter between targets and using intensity-modulation [6] or intensity-modulated arc therapy to treat multiple lesions simultaneously [8, 9]. The extreme of this method, and the method to be verified, uses a single isocenter and treats all lesions simultaneously

using multiple arcs. Dosimetry can be challenging for radiosurgery treatments due to small field sizes, high doses, and complex treatment geometries [10] and adding the complexities of volume modulated arcs and delivery to targets off isocenter increases the difficulty of verification even more.

1.4 Current Treatment Verification Techniques

Dose distributions can be clinically verified using 2D methods such as radiochromic film or diode arrays for relative dosimetry with absolute dose measurement points using ion chambers [11]. Gafchromic EBT2 film, a radiographic film, has been shown to provide high resolution 2D measured dose distributions without angle-dependent response [12]. The high resolution achievable with film is useful for radiosurgery treatments due to the steep drop-off of the dose around the target in these plans [13]. MapCheck (Sun Nuclear) is a 2D diode array used in routine IMRT QA for both relative and absolute measurements, providing similar results to film and ion chambers [14].

Delta4 (ScandiDos) is a unique device that provides more spatial information than film or a planar array. Two orthogonal diode arrays measure the dose at discrete points in two planes. The dose to regions between the diodes and even between the planes is calculated with an interpolation algorithm, providing a “pseudo” 3D

dosimetry technique. The system can also be calibrated to provide an absolute dose measurement to eliminate the need for an ion chamber reference [15].

1.5 Advantages and role of 3D Dosimetry

Using planar (2D) dose measurements for 3D dose verification can be time consuming and provides only a limited sampling of the true 3D distribution. IMRT plans are tested using film with all beams delivered at a gantry angle of zero, a method which fails to verify geometric accuracy of the treatment. Angular dependencies of planar methods, while minor, could also contribute to measurement error when verifying dynamic arc plans. The delta4 system relies on interpolation algorithms to generate 3D data. While the algorithm provides fairly accurate results [15], there are limitations to the gantry angles that can be measured. The ideal dosimetry method for complex IMRT and VMAT plans would have true 3D sampling to detect possible geometric inaccuracies during treatment, high spatial resolution for steep dose gradients, and fast acquisition time for a high patient load[16-18].

1.6 Scope and Aims of this work

The aims of this project are to provide verification for a multifocal radiosurgery treatment plan and to demonstrate the utility of PRESAGE as a reliable 3D dosimeter for complex treatments. The scope of the project includes delivery of the radiosurgery plan to the PRESAGE dosimeter, analysis of the PRESAGE formulation using cuvettes, and

comparison of the dose distribution delivered versus planned. A new method to scan highly attenuating dosimeters, which is directly applicable to measuring the high SRS doses, is also explored.

2. Methods

A RapidArc SRS plan was verified using an RPC-type head and neck phantom and five dosimeters. Due to the high prescription dose of the radiosurgery plan, dosimeters with reduced sensitivity were required. The prescription dose was scaled down for the first two dosimeters, which were more sensitive. The final three dosimeters were formulated with a significantly lower sensitivity and were treated with the full 20 Gy SRS prescription dose. The dosimeters were scanned using an optical-CT system and reconstructed to be compared to the Eclipse treatment plan. Even with a significantly lower sensitivity, the fully-dosed dosimeters turned very dark from irradiation. In order to avoid reconstruction attenuation artifacts and to improve the overall image quality for these scans, a new acquisition protocol was developed (section 2.3.4).

2.1 Multifocal RapidArc Treatment Planning

Due to the Novalis Tx being a joint venture between BrainLab and Varian, components from each company's treatment planning systems were used to develop a complete RapidArc SRS treatment plan for the machine [19].

2.1.1 iPlan

Localization of the tumors and placement of the isocenter were done using iPlan. A PRESAGE dosimeter in the head and neck phantom was scanned with the CT-simulator. The scan was exported into iPlan in order to add one central lesion and four

peripheral lesions and to place the isocenter over the central lesion. After the structures and isocenter were added, the plan was exported to Eclipse for arc optimization.

2.1.2 Eclipse

Each of the five arcs was added by inputting starting and ending gantry angles and using inverse planning to optimize the multi-leaf collimators. The orientation of the arcs, as well as the structures imported from iPlan, can be seen in the figure below in the Eclipse interface.

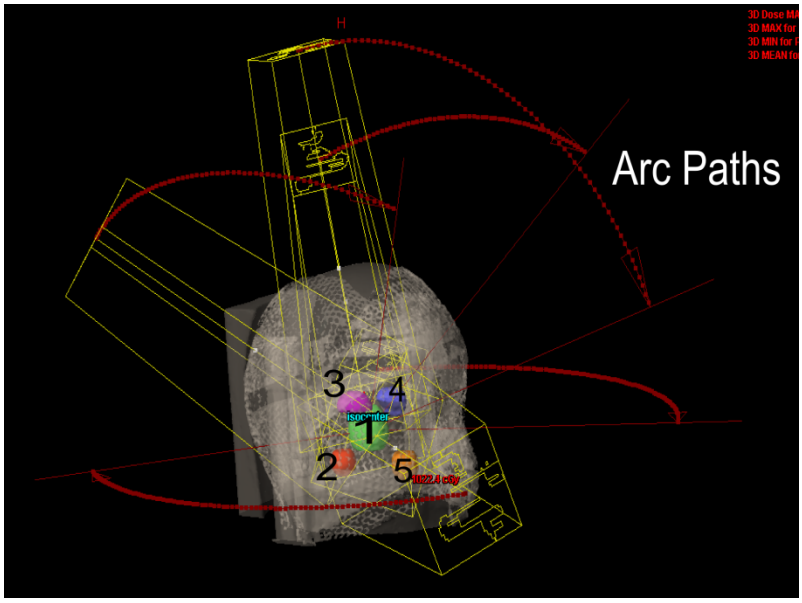

Figure 1: RapidArc SRS plan in Eclipse; the 5 arcs are shown in red and the five targets are labeled

2.2 Treatment Delivery

The treatment was delivered to a PRESAGE dosimeter in a head and neck phantom using a Novalis Tx machine. The treatment was delivered to five dosimeters as

well as an ion chamber embedded in a PRESAGE dosimeter in the same head and neck phantom. Delivery to the ion chamber provided an absolute dose reference point.

Figure 2: Novalis Tx at Duke University was used to deliver the SRS treatment

2.2.1 Immobilization and Positioning

Once the dosimeter was inserted into the phantom, the phantom was immobilized on the treatment couch using a thermoplastic mask and a SRS U-frame. Target positioning (TAPO) paper was used to properly align the phantom to the treatment isocenter. The positioning of the phantom was verified using the machine's on-board-imaging capabilities. The cone-beam CT image was registered to the simulation CT and when necessary, the isocenter was shifted. While the imaging dose to the dosimeter from the CBCT exists, it contributes less than 1% of the prescription dose and is deemed insignificant.

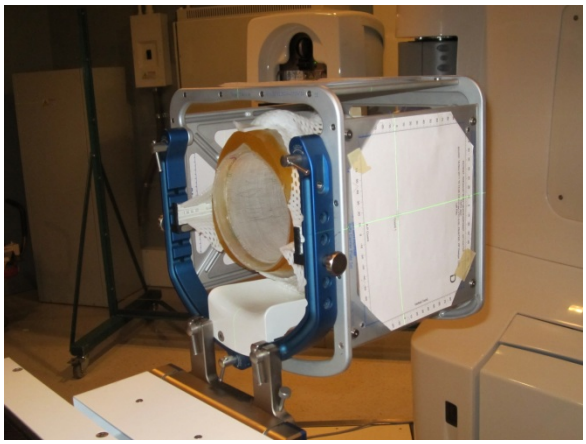

Figure 3: Head and neck phantom with target positioning paper and frame

2.2.2 Arc Set-Up and Beam On

Each of the five arcs was independently set up by adjusting the couch angle. While adjusting the couch angle in the treatment room, the gantry was rotated within the range of the arc to check for gantry-couch collisions. The collimator was set to 20° to prevent systematic accumulation of interleaf leakage from the tongue-and-groove effect along one plane. After the couch angle was adjusted, the other parameters were double checked from the treatment console and beam on was initiated.

2.2.3 Ion Chamber Absolute Dose Measurements

A SRS ion chamber was placed in a PRESAGE dosimeter in the head and neck phantom and treated with the multifocal SRS plan. The conventional -300 V bias was used when taking the measurement and leakage was accounted for by recording the time of each measurement. The dose measurement for each arc was summed up and compared to the Eclipse dose at the effective point of measurement to verify proper

delivery of the plan. In all cases, the measured dose was less than 0.5% off of the calculated Eclipse dose at the effective point of measurement.

2.3 Optical-CT Scanning and Reconstruction

PRESAGE dosimeters (Section 2.4) were scanned using two optical-CT systems developed in house: the Duke Medium-field optical scanner (DMOS) and the Duke Large-field optical scanner (DLOS). Both systems, while different in size, operate in a way similar to X-ray computed tomography, using visible light and a CCD camera instead of X-rays and detectors. Projections consisting of line integral values at each pixel are collected from different angles and used to reconstruct the dose distribution in three dimensions.

2.3.1 Duke Large-field Optical Scanner (DLOS)

The DLOS system uses a 3W LED light source behind a diffuser and a narrow band filter, giving the source a uniform flood field with wavelengths between 627 nm and 637 nm. Two 30 cm telecentric lenses provide a central region of parallel light where the dosimeter can be imaged free of object magnification effects. The imaging lens has a magnification of 0.037X and collimates any light with more than a 0.1 degree deviation from the optical axis, effectively minimizing scattered light contributions. A 1040x1392 CCD based Basler camera is used for imaging [20, 21]. The dosimeter is immersed in a fluid bath with a matched refractive index to minimize bending of the light at the

dosimeter-fluid interface. The dosimeter is placed on a motorized rotating stage in the bath, allowing projection images to be captured from any angle [22-27].

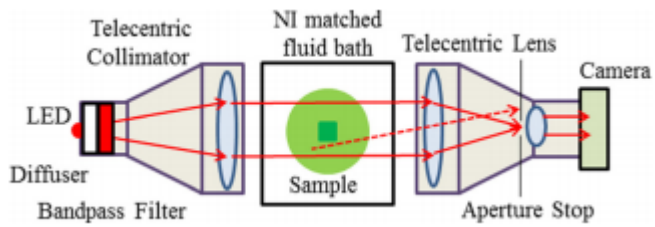

Figure 4: Diagram of DLOS system [20]

2.3.2 Pre and Post Irradiation Scanning

Since the change in optical density of the dosimeter is proportional to the dose, each dosimeter must be scanned before and after treatment in order to determine the change. Prior to pre-scanning, a plastic base is glued onto the base of the dosimeter. The base fits into the rotating stage of the optical-CT system in only one orientation, guaranteeing registration between pre and post scans. Each dosimeter was scanned in 1 degree increments with 360 degrees of rotation. To reduce noise, each projection was captured 25 times and averaged. After removing the dosimeter from the system, an image of the flood field was captured with 200 averages. The light source was then blocked to acquire a dark field with 200 averages. The optical density of the scan was calculated by subtracting out the background (dark) and normalizing by the flood to remove inhomogeneity, as shown in the equation below.

$$OD = \log\left(\frac{scan - dark}{flood - dark}\right)$$

The change in optical density was then calculated by dividing the pre scan value from the post scan value.

2.3.3 Reconstruction Algorithm and Filtering

Reconstruction was done using a MATLAB-based GUI (figure 5). The sinogram was generated using 1 mm resolution and a median filter of 5x5 or 10x10, depending on noise levels. The median filter reduced noise by taking the median value within a 5x5 (or 10x10) kernel surrounding a point and assigning it to that point. After the filtered sinogram was generated, the image was reconstructed with a length of 120 mm and a Ram Lak filter using MATLAB's iradon function.

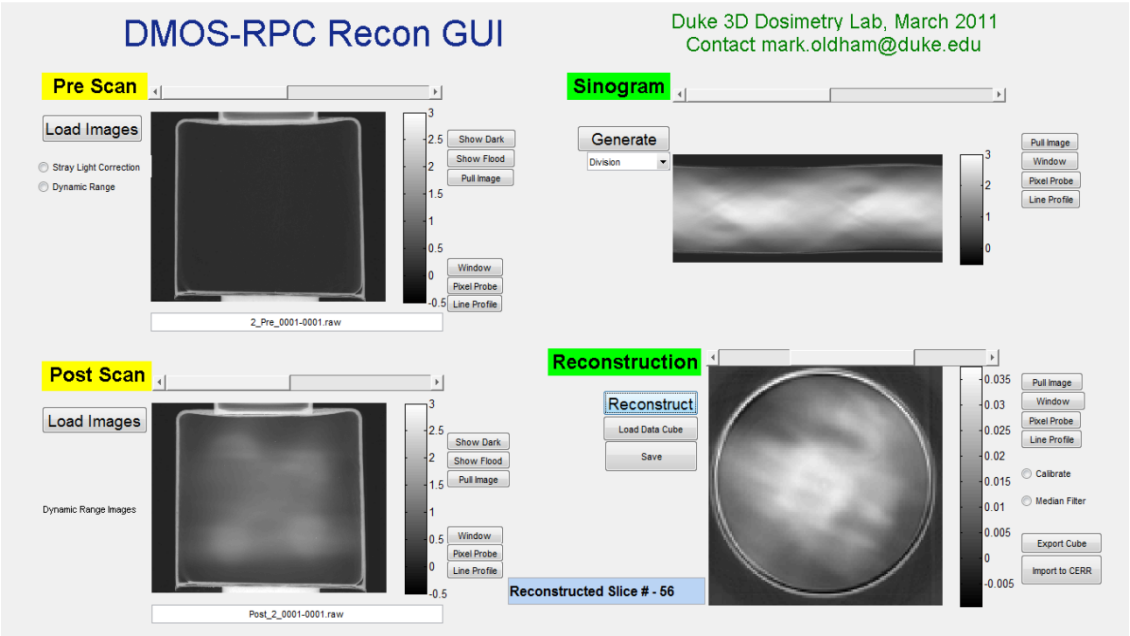

Figure 5: MATLAB-based reconstruction GUI; pre and post scans are loaded in in order to generate a sinogram and reconstruct the dose distribution

2.3.4 A Novel High Dynamic Range Technique for dark dosimeters

The amount of light counts in a line integral is dependent on attenuation and the integration time (shutter value) of the camera. The degree of attenuation is based on the path length and the optical density of the dosimeter. The integration time of the camera can easily be adjusted prior to scanning. To reduce noise and attenuation artifacts, it is ideal for all projections to have counts greater than 100. For a particularly dark dosimeter with low counts, the integration time can be increased. Eventually, increasing the integration time will saturate low attenuating regions at 4095 counts, particularly in the flood field surrounding the dosimeter. The scan cannot be accurately normalized by a saturated flood field.

The solution to this problem is to scan the dosimeter and acquire dark and flood fields at a standard integration time (~150) and also scan the dosimeter at a higher integration time. Assuming the amount of flood counts is proportional to the integration time (investigated and demonstrated in the results), the flood field can be scaled up by the ratio of the high and low integration times. A MATLAB algorithm searches through the high integration time projections and replaces saturated pixels with values from the scaled-up flood field at the same location. The scan can then be normalized by the scaled-up flood field.

2.4 PRESAGE 3D Dosimeters

PRESAGE is a radiochromic gel that consists of a melted polymer doped with leuco-malachite green, a chemical which changes conformation when exposed to ionizing radiation. The result is a color change from clear to green that is proportional to the dose delivered to the material [28]. Once the malachite green is added to the polymer, the mixture is set in a cylindrical shape to be used for 3D dosimetry. As the sensitivity, or optical density change per Gray, is dependent on the concentration of leuko-malachite green added to the polymer, each formulation of PRESAGE has a slightly different sensitivity [29, 30].

2.4.1 Dose Response

The main concern with planning a prescription dose for the radiosurgery plan is ensuring that the dosimeter is not overexposed from the treatment. If too much dose is delivered, the optical density change of the PRESAGE will be too large, resulting in projections with fully attenuated photons and zero counts. The result would be streak artifacts following reconstruction similar to those created by highly attenuating metal in X-ray CT scans.

The radiosurgery treatment was delivered to three formulations of PRESAGE. The first formulation was standard and had been used for lower dose irradiations. While doses around 20 Gy are typical for radiosurgery, the prescription had to be reduced to 5.5 Gy in order to avoid overexposure. The second formulation had roughly half the

sensitivity of the first formulation, allowing the prescription to be doubled to 11 Gy. The final formulation had less than half the sensitivity of the second formulation, allowing the full 20 Gy prescription dose without risking overexposure.

The sensitivity of each formulation was determined by irradiating 1 cm x 1 cm plastic cuvettes, filled with PRESAGE, to different doses using a standard treatment set up (section 2.4.2). A spectrophotometer (Genesys 20, ThermoSpectronic) was used to measure the optical density of each sample, using an empty cuvette as a zero. Cuvettes were scanned prior to the treatment and irradiated to various known doses before being re-scanned. A linear calibration curve was calculated by relating the optical density change to the delivered dose with the slope being the sensitivity.

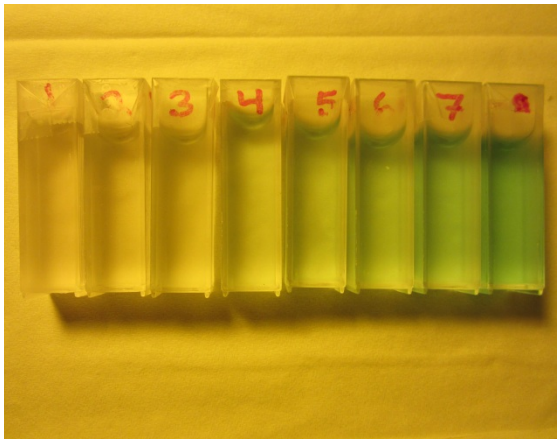

Figure 6: Cuvettes containing PRESAGE irradiated with doses of 0 to 25 Gy

2.4.2 Cuvette Irradiation

Each cuvette was treated with a 10x10 field at 100 cm SSD and a depth of 5.5 cm. The cuvette was placed in a 1 cm thick sheet of bolus material, with 10 cm of solid water below to allow backscatter and 5 cm of solid water above to achieve the 5.5 cm depth to

the center of the 1 cm cuvette. The treatment was delivered using 6 MV photons and a dose rate of 600 monitor units/min. With the field size and SSD set to calibration conditions, scatter factors were 1.00 and only the percent depth dose table was necessary to calculate the monitor units for the desired dose at 5.5 cm depth.

Table 1 Monitor units delivered to the D21 formulation cuvettes

Cuvette	*1*	*2*	*3*	*4*	*5*	*6*
Dose (Gy)	0	1	2.5	5	8	10
MU	0	118	295	590	944	1180

2.4.3 Temporal Stability of PRESAGE

Since previous formulations of PRESAGE have been known to drift in optical density over time, the optical density of each cuvette was measured immediately after treatment delivery, an hour after treatment delivery, and on a daily basis for at least a week to test stability. Cuvettes were stored in the freezer to improve stability by minimizing kinetic effects that could lead to optical density drift. To avoid direct temperature dependence effects while measuring optical density, cuvettes were taken out of the freezer 1-2 hours prior to being scanned each day.

2.5 Comparative Analysis of 3D Dose Distributions

Computation Environment for Radiotherapy Research (CERR) is a MATLAB tool developed at Washington University in St. Louis to analyze dose distribution in three dimensions[31]. Using CERR, the planned dose from Eclipse can be directly compared to the delivered dose via the reconstructed optical readout of the PRESAGE dosimeter.

2.5.1 Registration of measured dose to planned dose

The dose distribution of the plan (Eclipse) and the treatment (PRESAGE/Optical-CT) are oriented in different coordinate systems when initially imported into CERR. Before comparing the distributions in order to verify the treatment plan, the images must be registered. Image registration was performed using CERR's image fusion application using the Eclipse-planned dose as the base image and the delivered dose as the moving image. The images were roughly aligned by matching landmark structures in the dose distribution. Once the images were roughly aligned, fine registration was done by examining the dose profiles in all three planes and making minors shifts until all profiles matched. Once the first measured dose was registered to the plan, the same transform was used to register later distributions to the same orientation.

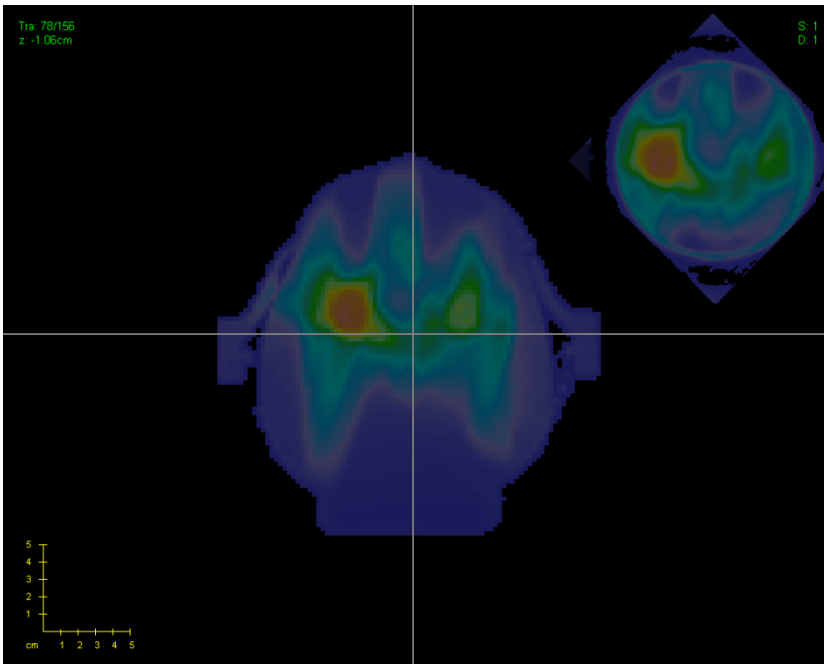

Figure 7: CERR's registration GUI; PRESAGE dosimeter (right) is registered to the Eclipse distribution (left) by matching the edges

2.5.2 Dose Normalization

The reconstructed optical-CT data considers attenuation of the dosimeter before and after the irradiation, resulting in values representing change in optical density. As the change in optical density is proportional to dose, a single absolute dose measurement can be used to scale the entire data set. The ion chamber measurement during treatment provided an absolute point dose for this purpose. The position of the effective point of measurement was determined from the CBCT image taken prior to treatment. Following image fusion of the treatment and plan, the optical density change was scaled to dose, using the ion chamber position as a reference.

2.5.3 Dose Volume Histogram and Gamma Analysis

Comparison of the delivered dose to the planned dose was done using two metrics. Dose volume histograms generated in CERR were used to separately evaluate treatment accuracy to each of the five lesions. Gamma analysis from a MATLAB algorithm was done to evaluate the overall agreement of the dose distributions. The gamma index takes both the different in dose and distance to agreement into account in one single metric.

$$\gamma(x_r, y_r) = \min\left(\Gamma_r(x_c, y_c)\right)$$

$$\Gamma_r(x_c, y_c) = \sqrt{\frac{\Delta r^2}{\Delta d_{max}^2} + \frac{\Delta D^2}{\Delta D_{max}^2}}$$

The Gamma value is calculated for a point in the reference dose distribution with respect to every point in the calculated dose distribution and the minimum of this collection of points becomes the gamma index for the given reference point. A point is considered to pass if its gamma index value is less than 1 [32]. The RPC credentialing criteria of 7% dose difference/4 mm distance-to-agreement, as well as the more stringent criteria of 5%/3 mm, and 3%/2 mm were used to analyze all dose distributions.

3. Results and Discussion

Results reported in this section include the outcomes of the cuvette irradiations of the three formulations of PRESAGE used in this experiment and the five dosimeters treated with the SRS plan. Results of the new high dynamic range scanning method are also reported.

Table 2: Overview of PRESAGE dosimeters irradiated in this work (D21, low sensitivity, and lowest sensitivity formulations)

Dosimeter ID	Formulation	Dose (cGy)	Sensitivity	OD change over time	5%/3mm pass
D21	D21	550	high	Increase	
LS1	Low sens.	1100	moderate	Stable	99.9
LS2a	Lowest sens.	2000	low	Decrease	85.6
LS2b	Lowest sens.	2000	low	Decrease	80.1
LS2c	Lowest sens.	2000	low	Decrease	84.0

3.1 PRESAGE sensitivity and temporal stabilities

The D21 formulation, standard and used in other experiments, and two lower sensitivity formulations (LS1 and LS2) were irradiated as described in section 2.4.2. In the following sections, the dose response, or sensitivity, of each formulation as well as the change in the sensitivity over time (stability) are reported.

3.1.1 Dose-Response

The D21 formulation had an initial sensitivity of 0.0225 change in OD/Gy/cm. The sensitivity was tracked daily over several weeks and found to increase to 0.0232 change in OD/Gy/cm two weeks after irradiation, a 3.1% increase. The sensitivity changes for all three formulations are presented in figure 11, normalized by the immediate measurements to quantify and compare stability.

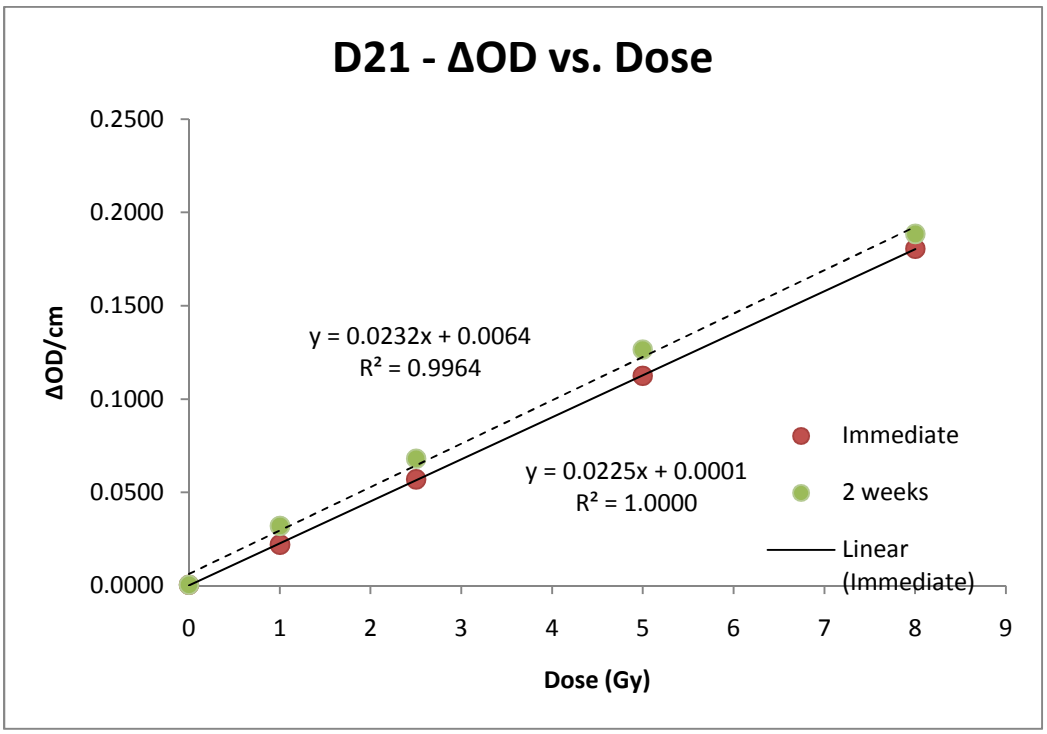

Figure 8: Dose response of the D21 formulation (high sensitivity)

The LS1 formulation had an initial sensitivity of 0.0102 change in OD/Gy/cm, which is 45% of the sensitivity of the standard D21 formulation. Such a reduction allowed the prescription dose to double without risk of overexposure of the dosimeter.

The sensitivity dropped to 0.0101 change in OD/Gy/cm several times over the period of two weeks before returning to its initial value of 0.0102.

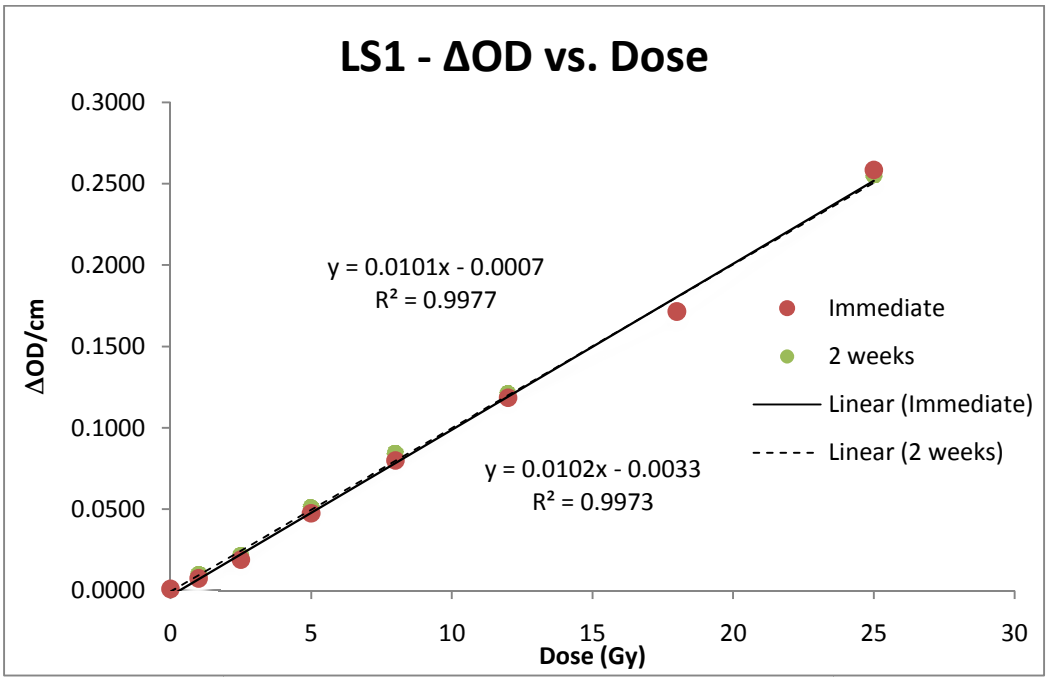

Figure 9: Dose response of the LS1 formulation (medium sensitivity)

The LS2 formulation had an initial sensitivity of 0.0047 change in OD/Gy/cm, a sensitivity 21% of the standard D21 formulation. By reducing the sensitivity even further than the LS1 formulation, the full 20 Gy prescription dose, typical of SRS treatments, could be delivered without risk of overexposure. The sensitivity of this formulation dropped by 10% to 0.0042 change in OD/Gy/cm over a week. The increased variation of the LS2 cuvette measurements compared to the previous formal could be the result of an

overall lower signal compared to the background noise of the spectrophotometer or simply a less stable formulation.

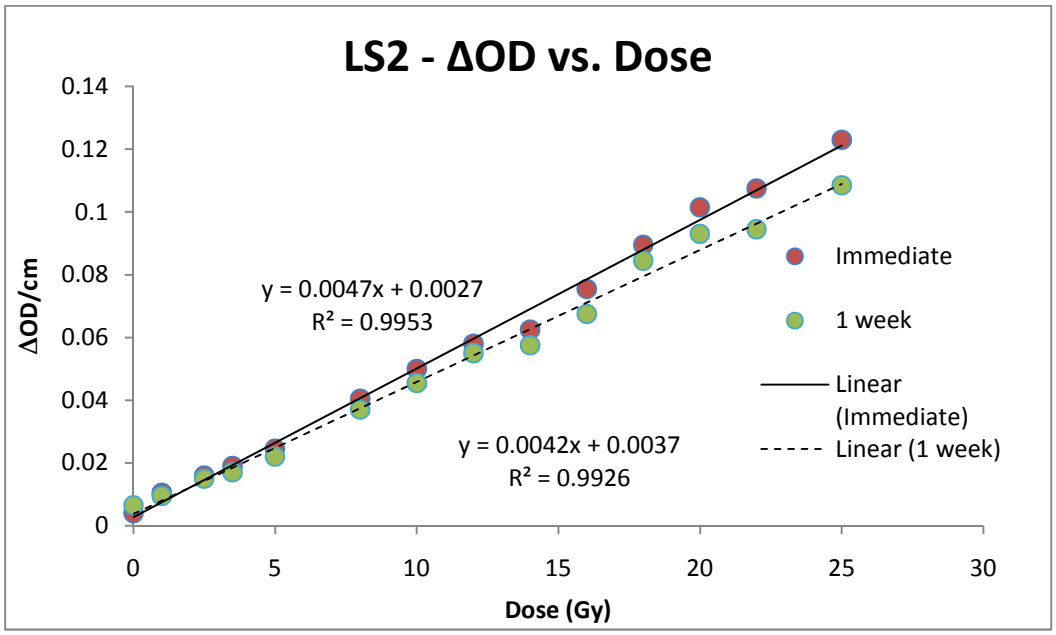

Figure 10: Dose response of the LS2 formulation (low sensitivity)

3.1.2 Stability

The difference in sensitivity of the three formulations is illustrated in Figure 11 as the measurements are tracked over time. In Figure 12, the sensitivity measurements are normalized by the initial value to examine the stability. By looking at the normalized plot, it is clear that the LS1 formulation was the most stable of the three, with less than 1% deviation in sensitivity in two weeks. The sensitivity of the LS2 formulation dropped by 10% in 5 days.

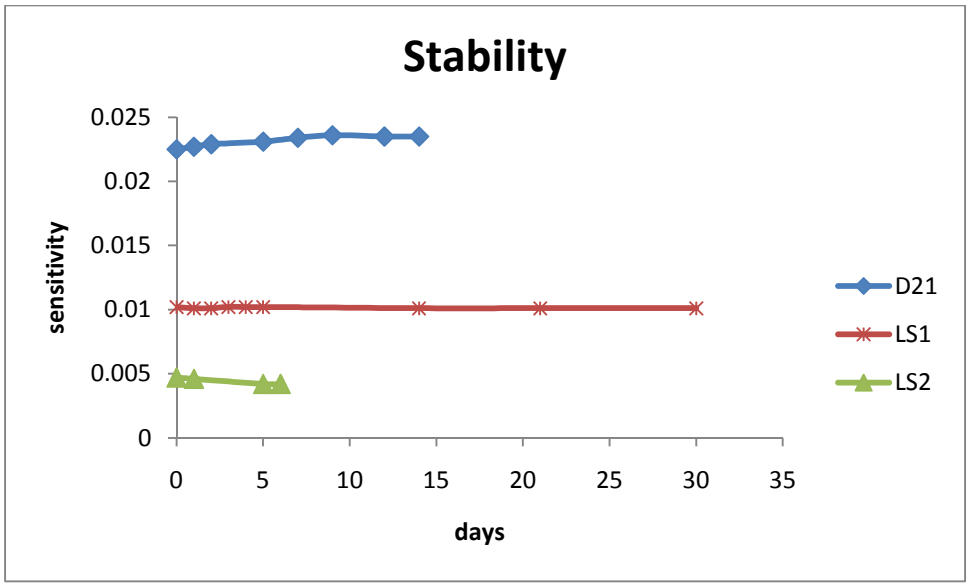

Figure 11: Sensitivity change over time of the three formulations

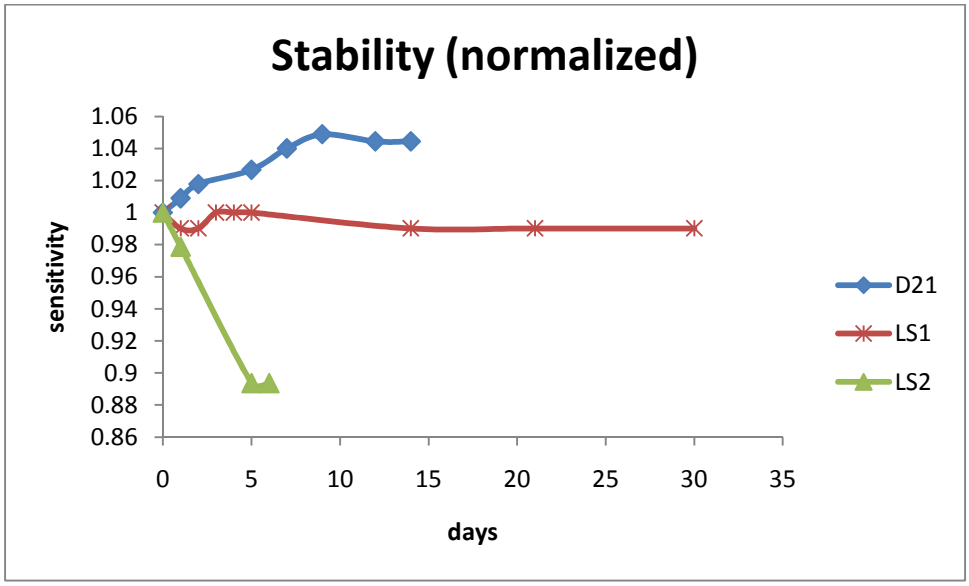

Figure 12: Normalized sensitivity change over time of the three formulations

3.2 Dosimeter Studies

In this section, the dose delivery measurements for LS1 and LS2 formulations are compared to the Eclipse-planned dose by specific target doses (minimum, maximum, mean dose, and dose volume histogram) and by overall distribution (gamma analysis). In 3.2.3, initial findings from the delivery to the D21 formulation are reported.

3.2.1 LS1 Formulation

The dose delivered to the LS1 formulation closely matched the Eclipse dose in the targets, with a less than 2% deviation in average dose to each target, and in the overall distribution with a Gamma passing rate (3% dose, 2 mm DTA) of 98.2%.

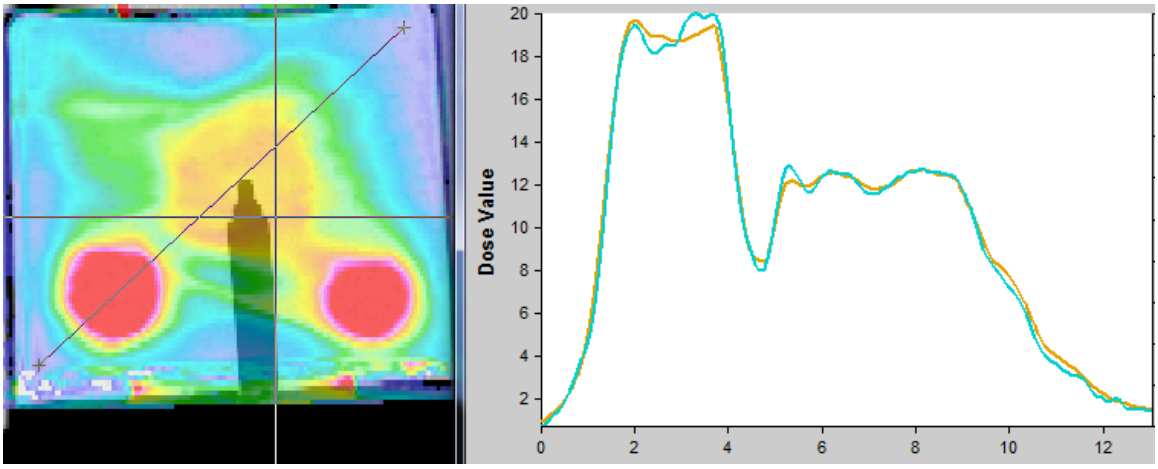

Figure 13: Dose profile through central and peripheral targets; Eclipse in yellow and LS1 delivery in blue

Table 3: delivered dose (Gy) to targets: LS1 vs. Eclipse dose

	Eclipse			LS1			
target	min	max	mean	min	max	mean	% difference
1	9.90	13.50	11.90	9.90	13.70	11.96	0.46
2	15.60	19.50	18.33	15.30	20.10	18.05	-1.53
3	14.50	19.50	18.32	14.70	19.70	17.98	-1.86
4	13.10	16.30	15.25	12.90	16.50	15.04	-1.35
5	14.10	20.10	18.42	14.10	21.10	18.59	0.92

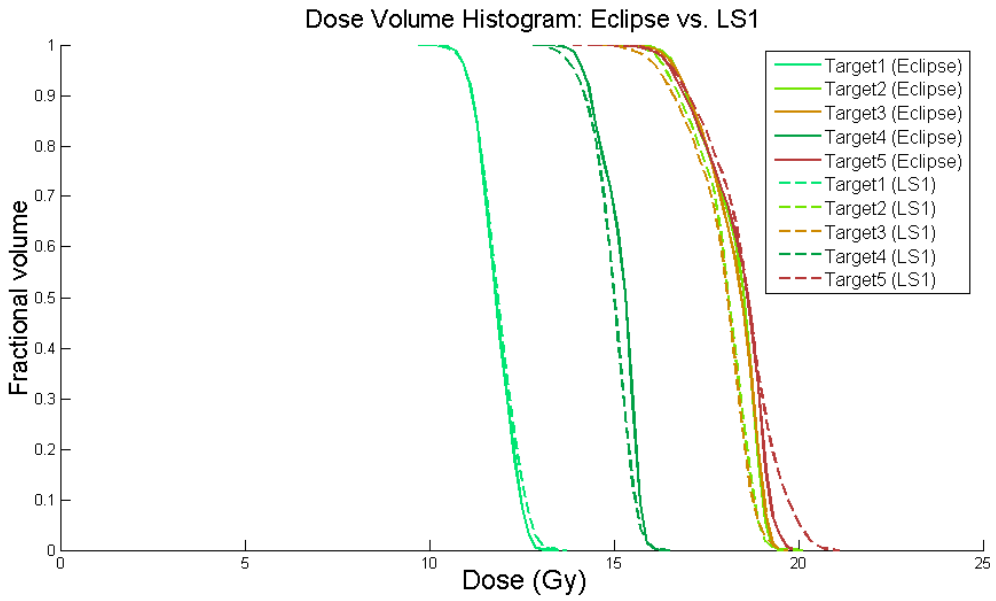

Figure 14: DVH for delivery to LS1 (dashed) vs. Eclipse (solid)

The dose volume histogram above shows excellent agreement between the planned and delivered doses with a slightly higher delivered dose in each target. Of all the targets, target 1 was most accurately delivered and measured compared to the planned dose. This could be attributed to the target's proximity to both the treatment isocenter and the absolute dose reference point to which the relative distribution of the

dosimeter is normalized. The small (<2%) deviation of average dose in the peripheral targets could therefore be attributed to either minor set-up errors (unlikely with CBCT verification) or a minor Eclipse dose calculation/delivery error such as inaccurate leaf motion. The few voxels that did fail in the 3%/2mm Gamma map were mostly located on the right side of the coronal plane, both in the peripheral target and the surrounding low dose regions. Such a systematic organization of failing pixels could possibly suggest a minor delivery error with one or more of the arcs.

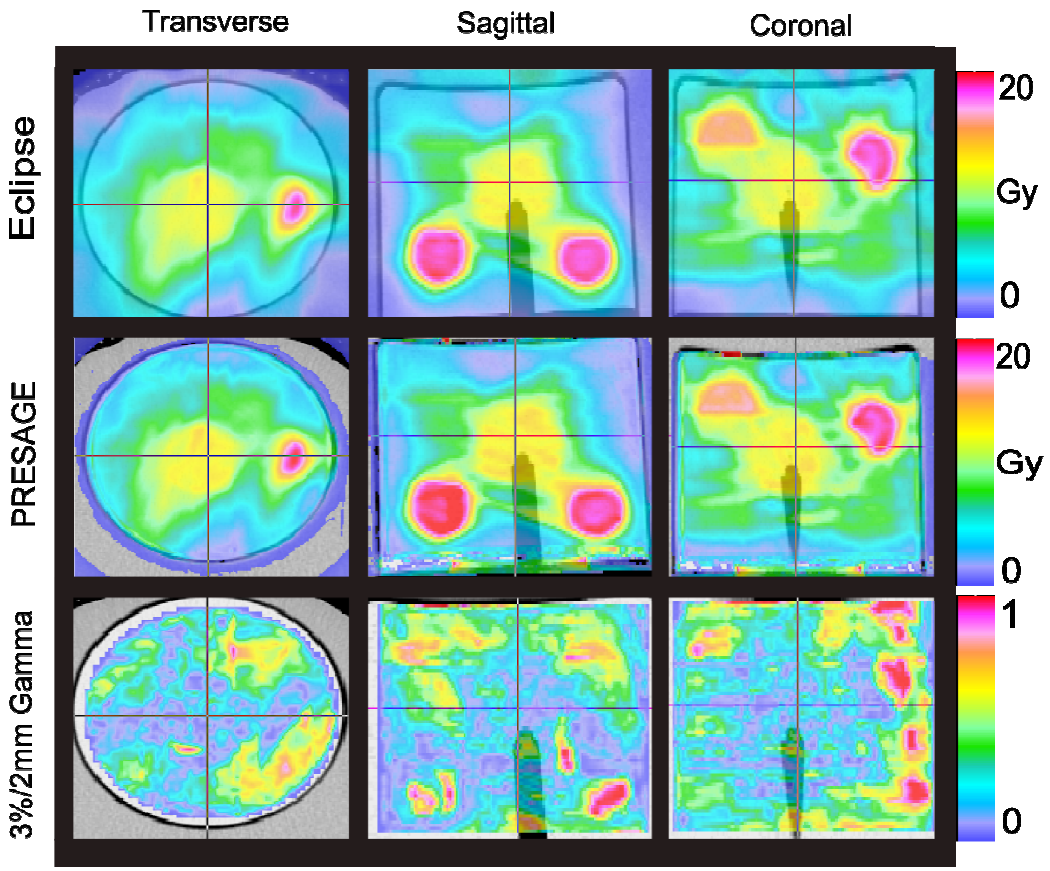

Figure 15: Eclipse plan compared to LS1 PRESAGE delivery with 3%/2 mm gamma map

A third possibility for the error could involve the dosimeter itself. Earlier formulations of PRESAGE (including the D21 formulation, see section 3.2.3) have suffered from various degrees of temporal instability. The optical density of the dosimeter can change over time, following exposure to radiation. While the LS1 formulation exhibited a high degree of stability in the cuvettes at all doses, temporal instability was observed in comparing later dosimeter measurements to immediate post-exposure measurements, and could play a role in the limited error observed on the Gamma map and dose volume histogram.

The dose-dependent instability was further investigated by irradiating a LS1 formulation dosimeter with a simple 5 field plan and measured at several times post irradiation. The optical density remained constant over three days in the 6 Gy region. The optical density dropped over time in the 12 and 19 Gy regions.

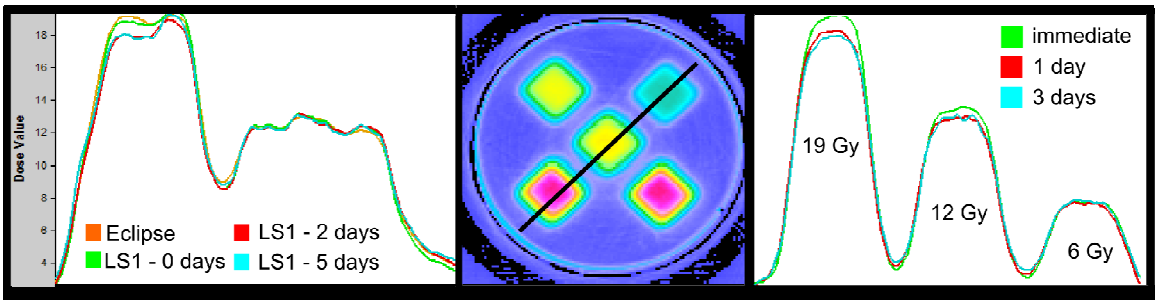

Figure 16: High dose regions drop over time (left); temporal instability dependent on dose (right)

3.2.2 LS2 Formulation

In all three LS2 dosimeters, targets 1, 2, and 5 had doses within 5% of the Eclipse plan. Targets 3 and 4, the peripheral targets at the top of the dosimeter had slightly more

error, ranging from 3.1% to 9.0% in target 3 and from 5.8% to 7.8% in target 4. The deviations in targets 3 and 4 are also evident in the dose volume histograms (Appendix A).

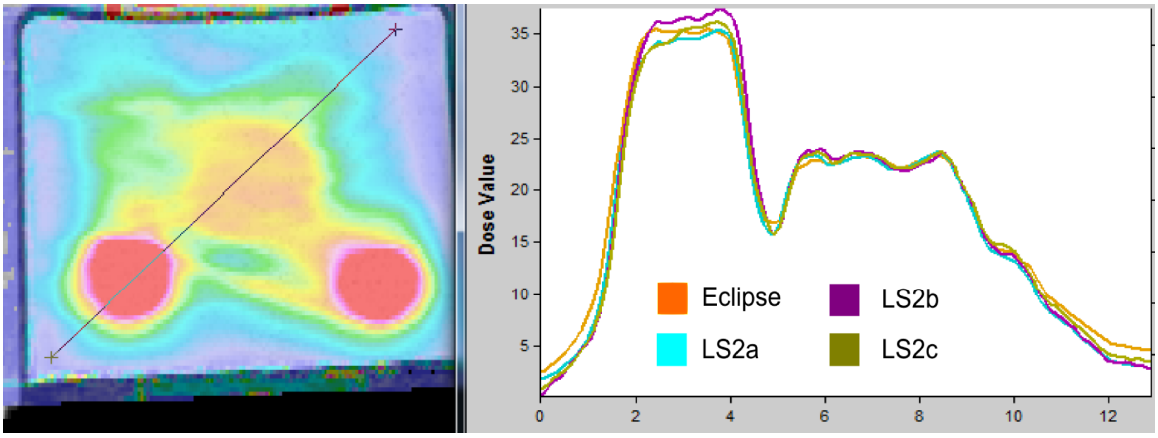

Figure 17: Dose profile through central and peripheral targets

Table 4: Delivered dose (Gy) to targets: LS2 dosimeters vs. Eclipse dose

	Eclipse			LS2a			
Target	min	max	mean	min	max	mean	% difference
1	18.5	24.9	22.0249	18.3	25.1	22.0566	0.1
2	28.9	36.3	33.9236	26.3	36.3	32.7164	-3.6
3	26.9	36.6	33.8972	23.1	34.9	30.8558	-9.0
4	24.3	30.3	28.2126	20.1	30.3	26.5838	-5.8
5	25.9	37.1	34.09	24.9	27.5	33.3849	-2.1

	Eclipse			LS2b			
Target	min	max	mean	min	max	mean	% difference
1	18.5	24.9	22.0249	17.3	28.1	21.9447	-0.4
2	28.9	36.3	33.9236	27.5	38.1	34.0018	0.2
3	26.9	36.6	33.8972	24.3	35.7	31.9185	-5.8
4	24.3	30.3	28.2126	20.5	29.9	26.4139	-6.4
5	25.9	37.1	34.09	24.9	39.9	34.9548	2.5

	Eclipse			LS2c			
Target	min	max	mean	min	max	mean	% difference

1	18.5	24.9	22.0249	17.9	25.3	22.0641	0.2
2	28.9	36.3	33.9236	25.5	36.3	33.0476	-2.6
3	26.9	36.6	33.8972	25.3	36.9	32.865	-3.1
4	24.3	30.3	28.2126	19.1	29.3	26.0226	-7.8
5	25.9	37.1	34.09	24.7	38.9	33.4492	-1.9

As expected, the results of the Gamma analysis were very dependent on the dose difference and distance-to-agreement criteria used. The LS2 formulation had a poor pass rate for the most stringent criteria but still managed to pass the RPC standard criteria of 7%/4 mm at a high rate. With the majority of the failing voxels being located on the periphery of the dosimeter, in both the targets and low dose regions of all three LS2 deliveries, the stability of the formulation is most likely the issue. This is supported by the cuvette results for the LS2 formulation, as the sensitivity dropped by 10% in 5 days. If the formulation is changing color at a dose dependent rate, scaling the relative distribution by the absolute reference point could easily cause the observed discrepancies in the regions dosed differently than the central target.

Table 5: Gamma passing rates for 3 sets of criteria

	Gamma passing rate		
	3%/2 mm	5%/3 mm	7%/ 4mm
LS1	98.2	99.9	100.0
LS2a	59.5	85.6	97.1
LS2b	52.0	80.1	96.9
LS2c	58.3	84.0	96.0

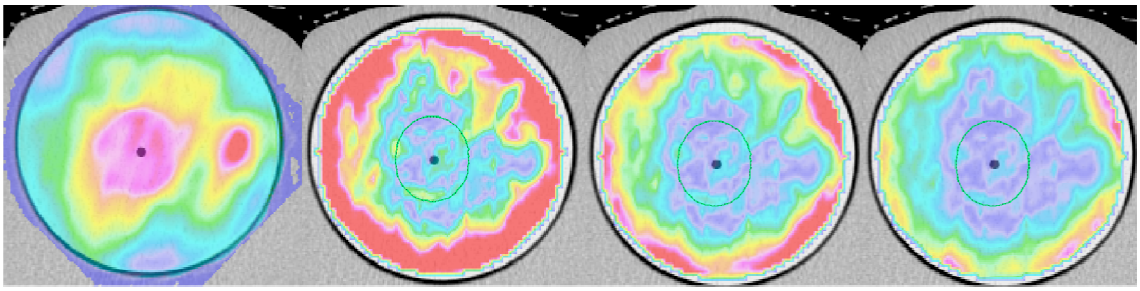

Figure 18: LS2a dose distribution (left) with gamma maps (3%/2mm, 5%/3mm, 7%/4mm)

3.2.3 D21 Formulation: Preliminary Results

The measured dose distribution of the delivery to the D21 formulation was not consistent with the Eclipse dose. While the central target and surrounding area matched within 1%, the measurement was significantly lower in the peripheral targets, with average doses differing by between 4.61% and 7.82%. Similar trends are evident in the dose volume histogram.

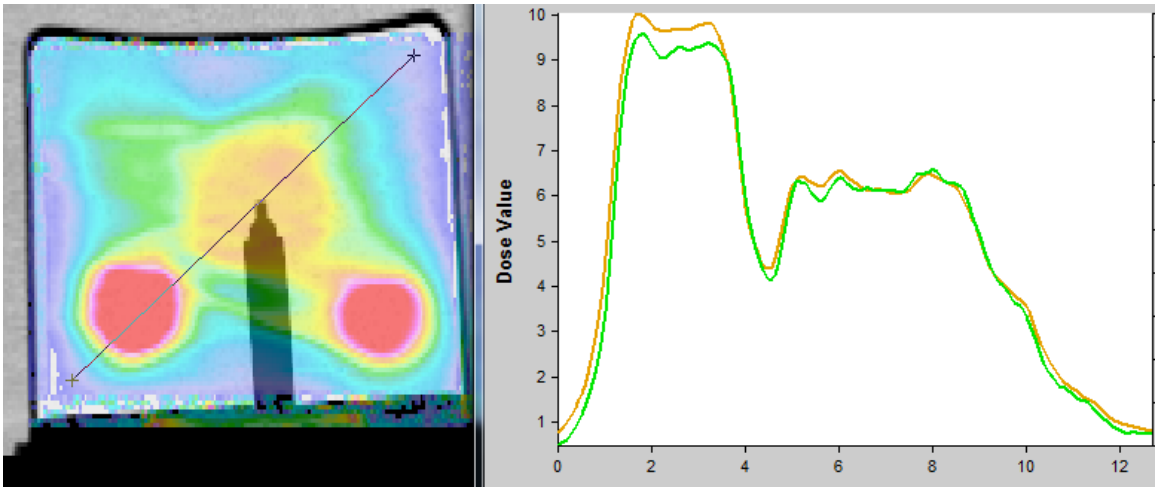

Figure 19: Dose profile through central and peripheral targets; Eclipse in yellow and D21 delivery in green

Table 6: delivered dose (Gy) to D21 vs. Eclipse dose

	Eclipse			D21			
Target	min	max	mean	min	max	mean	% difference
1	5.1	6.9	6.0579	4.7	6.9	6.0253	-0.54
2	8.1	9.9	9.3293	6.7	9.5	8.6975	-6.77
3	7.5	10.1	9.3246	6.7	9.7	8.7397	-6.27
4	6.9	8.3	7.7591	5.1	7.9	7.152	-7.82
5	7.1	10.1	9.3763	6.9	9.9	8.9443	-4.61

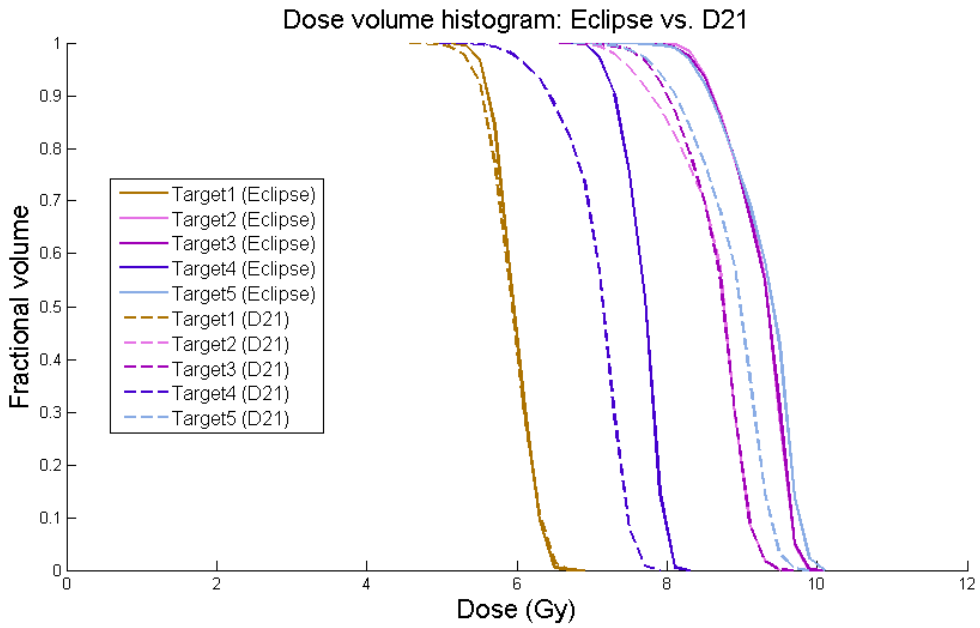

Figure 20: DVH for delivery to D21 (dashed) vs. Eclipse (solid)

It was hypothesized from these preliminary results that the PRESAGE formulation was suffering from a previously observed phenomenon, in which the dosimeter clears over time at a rate dependent on the dose delivered. Since the central target received a lower dose and the distribution was scaled to the ion chamber

reference point in the central target, the highly dosed regions would be underestimated when scaling. The figure below shows the long term effects of this dose related instability. The dose profile is normalized in the central region at the ion chamber location, resulting in consistent central dose. In the regions of higher and lower dose, the profile changes over time, particularly in the highly dosed peripheral target.

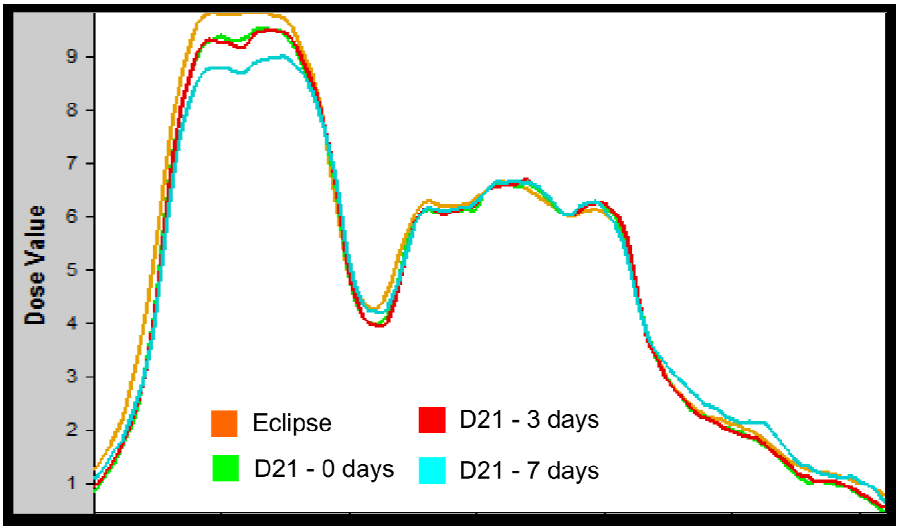

Figure 21: Dose dependent temporal instability in D21

3.3 High Dynamic Range scanning

Accurately extrapolating the number of flood counts based on the shutter value of the camera is conditional on the assumption that a linear relationship between both parameters exists. By measuring average counts in flood fields at different shutter values, this assumption was demonstrated.

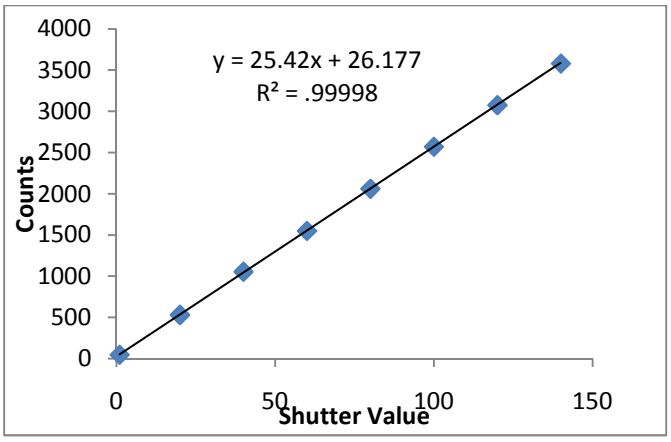

Figure 22: Linear relationship between counts and shutter value

The dose distributions of the delivery to the LS2a dosimeter were acquired using the standard and high dynamic range scanning methods and found to be consistent, with less than 1% average dose difference to each target. Due to the darkness of the irradiated LS2 dosimeters, acquiring accurate data was a concern. The fact that the standard method produced such similar results to the new method suggests that the dosimeters were not dark enough to cause reconstruction artifacts. This consistency also verifies the new method's accuracy in reconstructing moderately-attenuating dosimeters.

Table 7: Comparison of dose delivery using standard acquisition and high dynamic range acquisition for LS2a dosimeter

	Standard			HDR			
Target	min	max	mean	min	max	mean	% difference
1	18.5	25.1	22.1186	18.3	25.1	22.0306	0.40
2	26.3	36.1	32.6341	26.1	35.7	32.4322	-0.62
3	23.7	34.9	30.9166	23.7	34.5	30.7192	-0.64
4	20.5	30.1	26.6545	20.5	29.9	26.4515	-0.76
5	25.5	37.1	33.27	25.3	36.9	33.0286	-0.73

For an extremely dark dosimeter with a highly dosed central region, the high dynamic range scan removed attenuation streak artifacts and reduced noise. With the standard method, the number of counts in some of the projections was less than 50, approaching the background value for the scanner. By increasing the shutter value of the camera by over four times, the counts through the most attenuating region were brought back up to values above the background noise. The shutter value could be safely increased until the projection counts saturated, which did not occur even at a shutter value of 700. Using the standard method, the flood counts saturated before the shutter value reached 200.

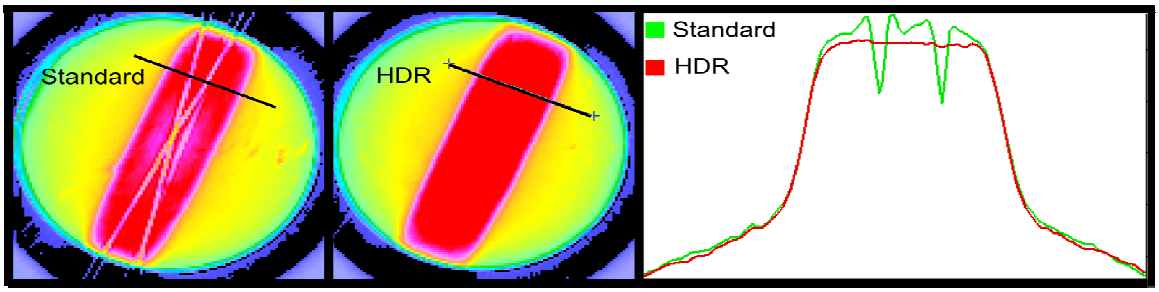

Figure 23: Dose distribution of standard and HDR method (left) and dose profile of standard and HDR methods (right)

4. Conclusions

The aims of the project were to provide a new method of verification for multifocal RapidArc radiosurgery plans, to demonstrate the use of PRESAGE/Optical-CT as a dosimetric technique for complex treatments, and to explore a new acquisition method for scanning highly attenuating dosimeters. Each of these aims was met to a certain degree with substantial room for future investigation.

The delivery to the LS1 formulation of PRESAGE closely matched the Eclipse planned dose, with a 3%/2 mm Gamma passing rate of 98.1% and was by far the most successful delivery. Such a high passing rate would be more than sufficient for pre-treatment quality assurance for a radiosurgery plan. The LS1 results not only provide verification for the multifocal radiosurgery plan, but also demonstrate the potential of PRESAGE as a 3D dosimeter in complex treatments.

With the positive results of the LS1 formulation, also came the somewhat negative results of the LS2 formulation. While only passing the RPC constraints of 7%/4 mm, obvious dosimetric errors were observed in the periphery of all three dosimeters. Since temporal instability was the likely cause of such errors, and one of the main pitfalls of some previous PRESAGE formulations, the solution is obvious. Replicating the stability observed in the LS1 formulation would likely result in similar passing rates.

The concern of overexposing dosimeters by delivering the high doses typical of radiosurgery plans inspired the development of a novel acquisition method to

drastically increase the dynamic range of the optical-CT scanner. The new method was tested on the radiosurgery-treated dosimeters, which turned out to be within acceptable attenuation levels for standard scanning techniques. The real niche of the new high dynamic range method was realized while scanning an extremely dark dosimeter and effectively reducing noise and removing attenuation streak artifacts present in the standard scan. Use of the new method could very well replace the current lab protocol of limiting delivered doses to prevent low count projections.

There are several future directions to expand on the results of this work. Replicating the LS1 formulation's temporal stability, not only for repeated verifications of the radiosurgery plan, but for any complex treatment has a high priority. Once a stable formulation is achieved, new plans can be verified by changing either the number of targets or their orientation in the brain. Similar plans could also be verified using the newly commissioned TrueBeam linear accelerators at Duke. The other important direction is to further explore the high dynamic range technique. Testing the method for a wide range of darkened dosimeters would indicate when the standard method begins to fail. Development of a graphical user interface (GUI) for the new method would improve efficiency of the necessary processing.

Appendix A: Additional Figures

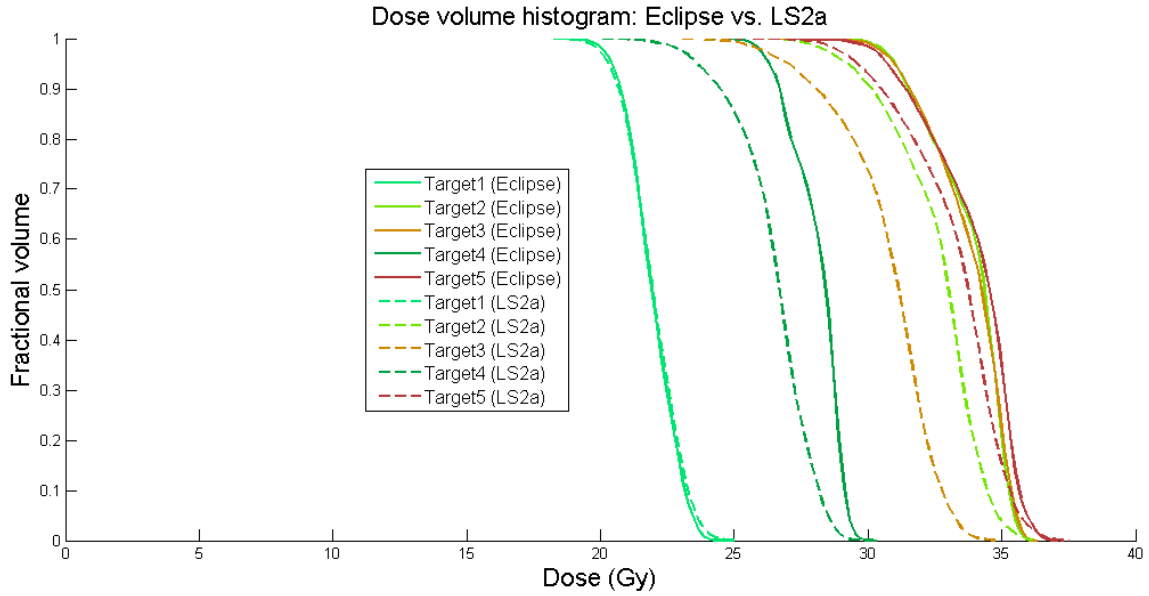

Figure 24: DVH for LS2a (dashed) vs. Eclipse (solid)

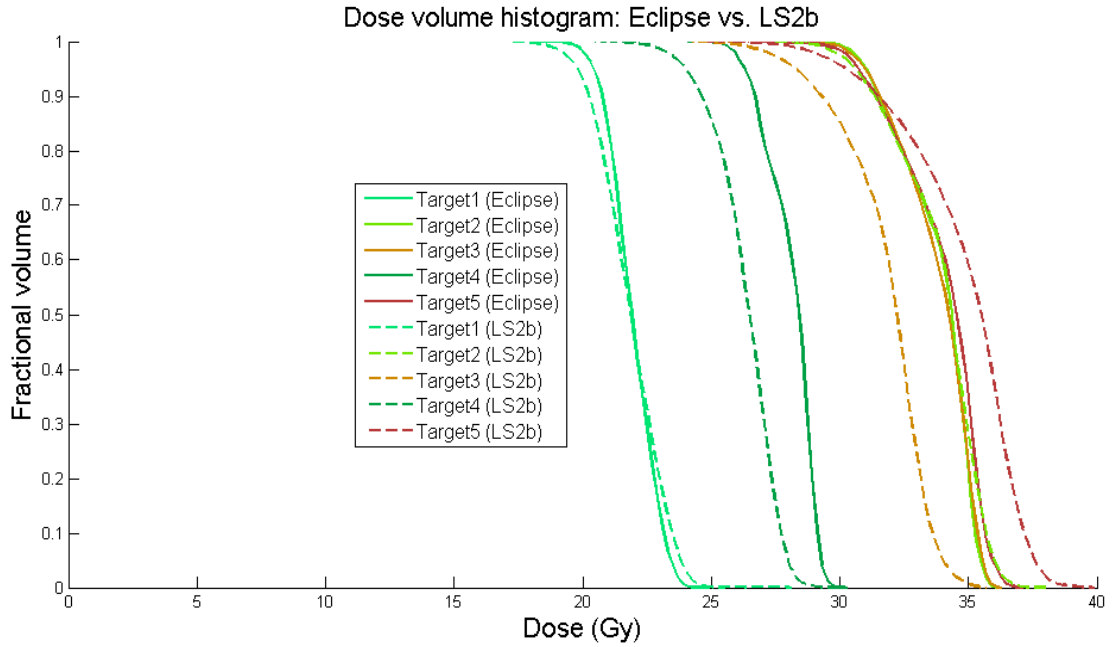

Figure 25: DVH for LS2b (dashed) vs. Eclipse (solid)

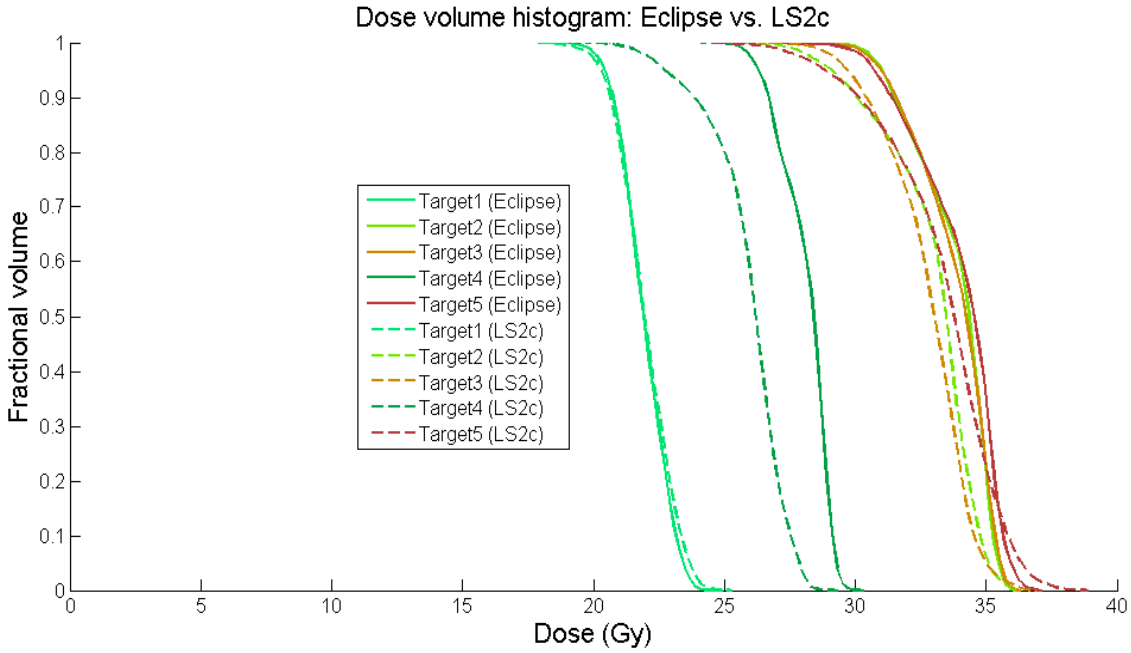

Figure 26: DVH for LS2c (dashed) vs. Eclipse (solid)

Appendix B: Abbreviation Key

SRS – Stereotactic Radiosurgery

SRT – Stereotactic Radiotherapy

IMRT – Intensity-modulated radiotherapy

VMAT – volume-modulated arc therapy

RPC – Radiological Physics Center

CT – computed tomography

CBCT – cone-beam computed tomography

DVH – dose volume histogram

CCD – charge-coupled device

DLOS – Duke Large-field Optical-CT Scanner

DMOS – Duke Medium-field Optical-CT Scanner

LS1 – low sensitivity formulation

LS2 – lowest sensitivity formulation

CERR - Computation Environment for Radiotherapy Research

HDR – high dynamic range

QA – quality assurance

DTA – distance to agreement

SSD – source-to-surface distance

OD – optical density

References

1. Schell, M.C., et al., *Stereotactic Radiosurgery: the report of AAPM Task Group 42.* 1995.

2. Benedict, S.H., et al., *Stereotactic body radiation therapy: the report of AAPM Task Group 101.* Med Phys, 2010. **37**(8): p. 4078-101.

3. Mack, A., et al., *Quality assurance in stereotactic radiosurgery/radiotherapy according to DIN 6875-1.* Stereotact Funct Neurosurg, 2004. **82**(5-6): p. 235-43.

4. Klein, E.E., et al., *Task Group 142 report: quality assurance of medical accelerators.* Med Phys, 2009. **36**(9): p. 4197-212.

5. Sankaranarayanan, V., et al., *Study on dosimetric parameters for stereotactic radiosurgery and intensity-modulated radiotherapy.* Med Dosim, 2003. **28**(2): p. 85-90.

6. Nath, S.K.L., J.D.; Simpson, D.R.; VanderSpek, L.; Wang, J.; Alksne, J.F.; Ciacci, J.; Mundt, A.J.; Murphy, K.T., *Single-Isocenter Frameless Intensity-Modulated Stereotactic Radiosurgery for Simultaneous Treatment of Multiple Brain Metastates: Clinical Experience.* Int. J. Radiation Oncology Biol. Phys., 2010. **78**(1): p. 91-97.

7. Roa, D.E., et al., *The use of RapidArc volumetric-modulated arc therapy to deliver stereotactic radiosurgery and stereotactic body radiotherapy to intracranial and extracranial targets.* Med Dosim, 2012.

8. Van Esch, A., et al., *Implementing RapidArc into clinical routine: a comprehensive program from machine QA to TPS validation and patient QA.* Med Phys, 2011. **38**(9): p. 5146-66.

9. Audet, C., et al., *Evaluation of volumetric modulated arc therapy for cranial radiosurgery using multiple noncoplanar arcs.* Med Phys, 2011. **38**(11): p. 5863-72.

10. Wang, Z., et al., *Dose Verification of Stereotactic Radiosurgery Treatment for Trigeminal Neuralgia with Presage 3D Dosimetry System.* J Phys Conf Ser, 2010. **250**(1).

11. Oldham, M., et al., *An investigation of the accuracy of an IMRT dose distribution using two- and three-dimensional dosimetry techniques.* Med Phys, 2008. **35**(5): p. 2072-80.

12. Kairn, T., et al., *EBT2 radiochromic film for quality assurance of complex IMRT treatments of the prostate: micro-collimated IMRT, RapidArc, and TomoTherapy.* Australas Phys Eng Sci Med, 2011. **34**(3): p. 333-43.

13. Wilcox, E.E. and G.M. Daskalov, *Evaluation of GAFCHROMIC EBT film for Cyberknife dosimetry.* Med Phys, 2007. **34**(6): p. 1967-74.

14. Letourneau, D., et al., *Evaluation of a 2D diode array for IMRT quality assurance.* Radiother Oncol, 2004. **70**(2): p. 199-206.

15. Sadagopan, R., et al., *Characterization and clinical evaluation of a novel IMRT quality assurance system.* J Appl Clin Med Phys, 2009. **10**(2): p. 2928.

16. Guo, P., J. Adamovics, and M. Oldham, *A practical three-dimensional dosimetry system for radiation therapy.* Med Phys, 2006. **33**(10): p. 3962-72.

17. Sakhalkar, H.S. and M. Oldham, *Fast, high-resolution 3D dosimetry utilizing a novel optical-CT scanner incorporating tertiary telecentric collimation.* Med Phys, 2008. **35**(1): p. 101-11.

18. Oldham, M., *Optical-CT scanning of polymer gels.* J Phys Conf Ser, 2004. **3**: p. 122-135.

19. Chang, Z., et al., *Dosimetric characteristics of novalis Tx system with high definition multileaf collimator.* Med Phys, 2008. **35**(10): p. 4460-3.

20. Thomas, A., et al., *Commissioning and benchmarking a 3D dosimetry system for clinical use.* Med Phys, 2011. **38**(8): p. 4846-57.

21. Thomas, A. and M. Oldham, *Fast, large field-of-view, telecentric optical-CT scanning system for 3D radiochromic dosimetry.* J Phys Conf Ser, 2010. **250**(1): p. 1-5.

22. Thomas, A., J. Newton, and M. Oldham, *A method to correct for stray light in telecentric optical-CT imaging of radiochromic dosimeters.* Phys Med Biol, 2011. **56**(14): p. 4433-51.

23. Thomas, A., et al., *A method to correct for spectral artifacts in optical-CT dosimetry.* Phys Med Biol, 2011. **56**(11): p. 3403-16.

24. Sakhalkar, H.S., et al., *A comprehensive evaluation of the PRESAGE/optical-CT 3D dosimetry system.* Med Phys, 2009. **36**(1): p. 71-82.

25. Sakhalkar, H., et al., *Investigation of the feasibility of relative 3D dosimetry in the Radiologic Physics Center Head and Neck IMRT phantom using presage/optical-CT.* Med Phys, 2009. **36**(7): p. 3371-7.

26. Sakhalkar, H., et al., *Investigating the Feasibility of 3D Dosimetry in the RPC IMRT H&N Phantom.* J Phys Conf Ser, 2009. **164**(2009): p. 12058.

27. Clift, C., et al., *Toward acquiring comprehensive radiosurgery field commissioning data using the PRESAGE/optical-CT 3D dosimetry system.* Phys Med Biol, 2010. **55**(5): p. 1279-93.

28. Guo, P.Y., J.A. Adamovics, and M. Oldham, *Characterization of a new radiochromic three-dimensional dosimeter.* Med Phys, 2006. **33**(5): p. 1338-45.

29. Pierquet, M., et al., *An investigation into a new re-useable 3D radiochromic dosimetry material, Presage.* J Phys Conf Ser, 2010. **250**(1): p. 1-4.

30. Brown, S., et al., *Radiological properties of the PRESAGE and PAGAT polymer dosimeters.* Appl Radiat Isot, 2008. **66**(12): p. 1970-4.

31. Deasy, J., *Computational Environment for Radiotherapy Research*, 2010: St. Louis, MO.

32. Low, D.A., et al., *A technique for the quantitative evaluation of dose distributions.* Med Phys, 1998. **25**(5): p. 656-61.